Supporting Online Material for

Elastic coupling between RNA degradation and unwinding by an exoribonuclease

Gwangrog Lee,[1,2] Matthew Bratkowski,[3] Fang Ding,[3] Ailong Ke,[3] Taekjip Ha[1,4]

1. Department of Physics, University of Illinois at Urbana-Champaign, 1110 West Green Street, Urbana, Illinois 61801, USA.
2. School of Life Sciences, Gwangju Institute of Science and Technology, Gwangju 500-712, Korea
3. Department of Molecular Biology and Genetics, Cornell University, Ithaca, NY 14853
4. Howard Hughes Medical Institute, Urbana, Illinois 61801, USA.

Material and Methods

RNA substrate preparation:
3’ RNA strands and chimeric DNA/RNA strands that are degraded by Rrp44 in the single molecule FRET measurements were purchased from Dharmacon. 5’ strands that are complementary to a portion of the 3’ strands were purchased from IDT DNA Technologies. The sequences and modifications are shown below.

1. GC-rich construct (60%): Fig. 1-2, Fig. 3, Fig. S1-2 and Fig S4
3’strand:
5’Biotin-UGG CGA CGG CAG CGA GGC ***5NU (Cy5)***CU CCC CAC CAC CAU CAC UUG GUC GAA AAA AAA AAA AAA A-3’ (Dharmacon)

5’ strand:
5’-***amino modifier C6 (Cy3)***-CGA CCA AGU GAU GGU GGU GGG GAG AGC CUC GCU GCC GUC GCC A 3’ (IDT DNA Technologies)

2. Chimeric-construct1 (7 nt chimera): Fig. S6-7
3’ chimeric strand: 5’-Biotin-18D-Cy5-18D-7R-15RA_tail:
5’Biotin-dTdGdG dCdGdA dCdGdG dCdAdG dCdGdA dGdGdC ***5NU (Cy5)***dCd**T** dCdCdC dCdAdC dCdAdC dCdAdT dCdAdC UUG GUC GAA AAA AAA AAA AAA A-3’ (Dharmacon)

5’ strand:
5’-***amino modifier C6 (Cy3)***-CGA CCA AGU GAU GGU GGU GGG GAG AGC CUC GCU GCC GUC GCC A 3’ (IDT DNA Technologies)

3. Chimeric-construct2 (15 nt chimer): Fig. S6
3’ chimeric strand: 5’-Biotin-18D-Cy5-10D-15R-15RA_tail:
5’Biotin-dTdGdG dCdGdA dCdGdG dCdAdG dCdGdA dGdGdC ***5NU (Cy5)***dCd**T** dCdCdC dCdAdC dCAC CAT CAC UUG GUC GAA AAA AAA AAA AAA A-3’ (Dharmacon)

5’ strand:
5’-***amino modifier C6 (Cy3)***-CGA CCA AGU GAU GGU GGU GGG GAG AGC CUC GCU GCC GUC GCC A 3’ (IDT DNA Technologies)

4. GA-only construct: Fig. S5
3’ strand:
5’Biotin- CUC UCU CCU CUC UCC UCC ***5NU (Cy5)*** CU CCU CUC CUC UCU CUC UCU CUC CAA AAA AAA AAA AAA A -3’ (Dharmacon)

5’ RNA strand:
5’-***amino modifier C6 (Cy3)***- GGA GAG AGA GAG AGA GGA GAG GAG AGG AGG AGA GAG GAG AGA G 3’ (IDT DNA Technologies)

5. RNA-DNA hybrid-construct: Fig. S10 and S11
3’ strand:
5’Biotin-UGG CGA CGG CAG CGA GGC ***5NU (Cy5)***CU CCC CAC CAC CAU CAC UUG GUC GAA AAA AAA AAA AAA A-3’ (Dharmacon)

5’ DNA strand:
5’-***amino modifier C6 (Cy3)***-dCdGdA dCdCdA dAdGdT dGdAdT dGdGdT dGdGdT dGdGdG dGdAdG dAdGdC dCdTdC dGdCdT dGdCdC dGdTdC dGdCdC dA-3’ (IDT DNA Technologies)

6. AU-rich construct: Fig. 3 and Fig. S12
3’ strand:
5’Biotin-UGG CGA CGG CAG CGA GGC ***5NU(Cy5)***UA UAA AUU AAU AAA UAU AUA AUU AUU UUU UUU UUU UUU U (Dharmacon)

5’ strand:
5’-***amino modifier C6 (Cy3)***-UAA UUA UAU AUU UAU UAA UUU AUA AGC CUC GCU GCC GUC GCC A 3’ (IDT DNA Technologies)

7. Gel construct: Fig. S3
3’ strand:
5’- UGG CGA CGG CAG CGA GGC ***5NU (Cy5)***CU CCC CAC CAC CAU CAC UUG GUC GAA AAA AAA AAA AAA A-3’ (Dharmacon)

5’ DNA strand:
5’-***amino modifier C6 (Cy3)***-dCdGdA dCdCdA dAdGdT dGdAdT dGdGdT dGdGdT dGdGdG dGdAdG dA-3’ (IDT DNA Technologies)

7. Gel construct: Fig. S9
3’ strand: (crossed linked construct)
5’-CUC UCU CCU CUC UCC UCC UCU CCU CUC CUC UCU CUC UCU CUC ***5NU (amino-crosslinker)*** A AAA AAA AAA AAA AA (Dharmacon)

5’ strand: (crossed linked construct)
5’-***Thio-modifier C6-s-s*** - AGA GAG AGA GAG AGA GGA GAG GAG AGG AGG AGA GAG GAG AGA G 3’ (IDT DNA Technologies)

3’ strand: (3 nt tail construct)
5’Biotin-UGG CGA CGG CAG CGA GGC ***5NU (Cy5)***CU CCC CAC CAC CAU CA C UUG GUC GAA A (Dharmacon)

5’ strand: (3 nt tail construct)
5’-***amino modifier C6 (Cy3)***-CGA CCA AGU GAU GGU GGU GGG GAG AGC CUC GCU GCC GUC GCC A 3’ (IDT DNA Technologies)

3’ strand: (5 nt tail construct)
5’Biotin-UGG CGA CGG CAG CGA GGC ***5NU (Cy5)***CU CCC CAC CAC CAU CA C UUG GUC GAA AAA (Dharmacon)

5’ strand: (5 nt tail construct)
5’-***amino modifier C6 (Cy3)***-CGA CCA AGU GAU GGU GGU GGG GAG AGC CUC GCU GCC GUC GCC A 3’ (IDT DNA Technologies)

Positions of internal modifications are marked in ***italic bold (5NU* and *amino modifier C6)***. Cy3 with a NHS ester (GE Healthcare, NJ) was attached to a C6 amino linker at the 5’ end of the 5’ strand whereas Cy5 was attached to a C4 amino linker at the base of a rU at an internal position of the 3’ strand, respectively. The labeling protocol was based on the single-molecule techniques laboratory manual (*31*). Briefly, 5 nmoles of RNA oligo in 35 μl of 50 mM sodium tetraborate buffer pH 8.5 was incubated with 50 nmoles of Cy3 or Cy5 by shaking overnight at room temperature. The labeled oligonucleotides were first purified by ethanol precipitation to remove unreacted dyes and then further purified by denaturing PAGE. RNA duplex constructs were annealed by heating a tube that contained the 3’ and 5’ strands to 90˚C for 5 minutes at micromolar concentrations with a molar ratio of 1:1.5 in 10 mM Tris-HCl and 50 mM NaCl pH 8.0, and then slowly cooling for 2-3 hours to room temperature.

Protein purifications: Wild type Rrp44 and mutant proteins were purified following the published protocols(*6*). Wild type Rrp44 full length (amino acids 1-1001) and Rrp44 ΔPIN (amino acids 270 – 1001) from *S. cerevisiae* were expressed in a ligation independent cloning vector containing an N-terminal 6Xhistidine tag by induction at 18 °C with 1 mM IPTG. Proteins were then purified using nickel chelation affinity chromatography with His-Select resin (Sigma-Aldrich). Rrp44 D171N and Rrp44 D171N, D551N were generated using site directed mutagenesis and purified in similar manner. RNase R was purchased from Epicentre® (an Illumina® company, catalog #: RNR07250).). We obtained the same step-wise unwinding behavior using Rrp44 further purified on monoQ column after the Ni-NTA chromatography. No RNase activity was detected from the Rrp44 D171N, D551N mutant protein purified using the one-step or two-step purification scheme, suggesting that contamination from unrelated RNases is not a concern.

Single-molecule FRET measurement.
RNA substrates (~100 pM) were immobilized with biotin-neutravidin interaction on polyethylene glycol (PEG) coated quartz slides in a reaction chamber to minimize nonspecific surface adsorption of proteins (*31*). The immobilized RNA substrates were incubated with either the Rrp44 protein (~30 nM) or RNase R (~10 nM) for ~2 minutes in an imaging buffer (20 mM Tris-HCl, pH 7.8; 15 mM NaCl; 1 mM DTT; 5 mM EDTA; 1 mg/ml BSA). An oxygen scavenger system (0.8% Glucose, 1 mg/ml glucose oxidase and 40 μg/ml catalase) and a reducing reagent (2 mM Trolox) were included in the imaging buffer to minimize photobleaching and blinking. The reaction is triggered upon addition of the same imaging buffer containing 100 μM $MgCl_2$ into the reaction chamber but omitting the protein and EDTA. All measurements were carried out at the room temperature (23 ºC) unless otherwise mentioned.

Single-molecule data acquisition.
FRET images were taken with the integration time of 30 and 100 milliseconds (33 Hz and 10 Hz frame rates, respectively) on a prism-type total internal reflection fluorescence (TIRF) microscope equipped with an Andor EMCCD camera. The donor Cy3 was excited by an Nd:YAG laser (532 nm,75 mW, crystal laser). Fluorescence signal passing through a water immersion objective lens (603, Olympus) was filtered out through a 550 nm long-pass mirror to block out laser scattering. The emissions from the donor and acceptor were then split using a 630 nm dichroic mirror and imaged onto the two halves of the camera. The acquisition was controlled using a user interface written in Visual C++. The reaction was triggered while video images were being taken by the camera. The recorded video files were processed to extract single-molecule traces by custom scripts written in IDL.

Single-molecule data analysis.
FRET efficiency is defined as the fluorescence intensity of the acceptor divided by the sum of intensities of the donor and acceptor. Analysis on individual FRET-time traces was performed using Origin or programs written in Matlab. Histograms of single molecule FRET efficiency were built from hundreds of RNA molecules using an automated program by selecting fluorescent spots within an intensity range defined to avoid the selection of spots arising from fluorescent impurities. The dwell time of each step from FRET and time traces were determined using a step finder program used previously (*9, 19*).

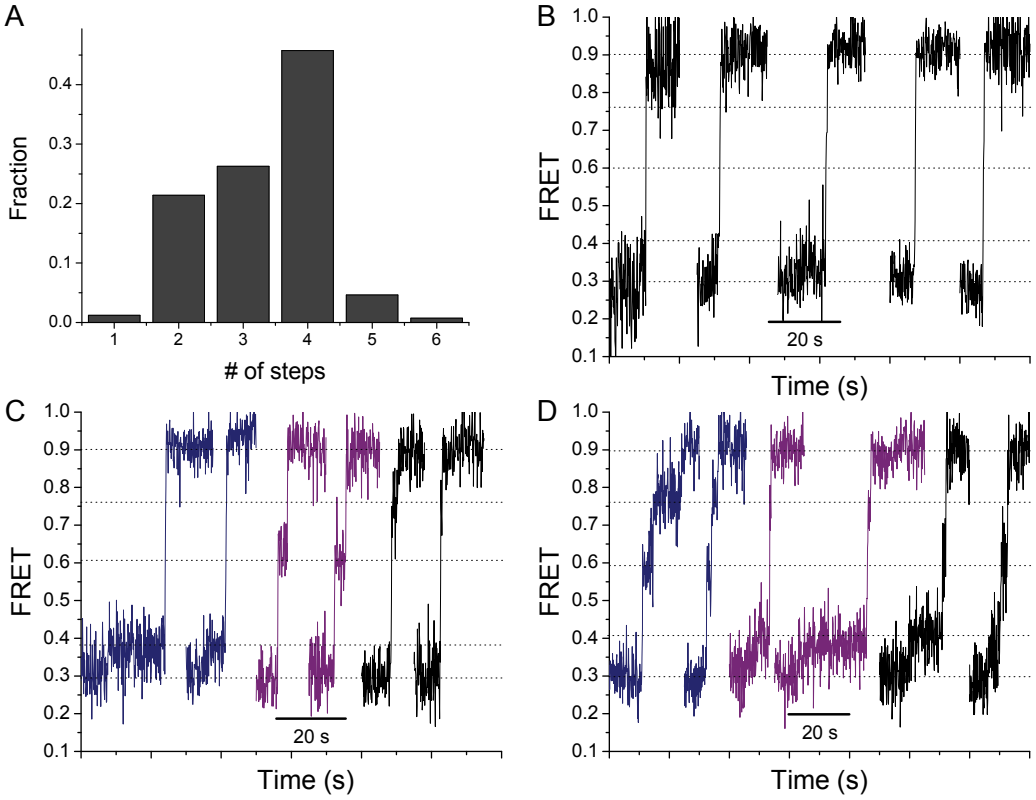

Fig. S1. Diverse stepping behaviors of Rrp44-induced unwinding of RNA. The number of steps during unwinding vary from 1 to 6 for degradation of the standard RNA substrate (60% GC content). The most frequent is the four steps pattern as shown in Fig. 1 (45% of total population). The steps in molecules showing 2 or 3 steps appear at well-defined FRET values also shown in 4 steps traces (marked by horizontal dotted lines), indicating that fewer than 4 steps are due to steps that are too brief to be detected. (A) A distribution of the number of steps. (B) Representative traces showing the one step pattern (~1.2 %) where no intermediate is seen. (C) Representative traces showing the two-step pattern (21%) where two of the three intermediate pauses are missing. (D) Representative traces showing the three-step pattern (26%) where one of the three intermediate pauses is missing. Most traces show very discrete steps even if pauses are sometimes missing. Less than 5% of the traces showed more than 4 steps.

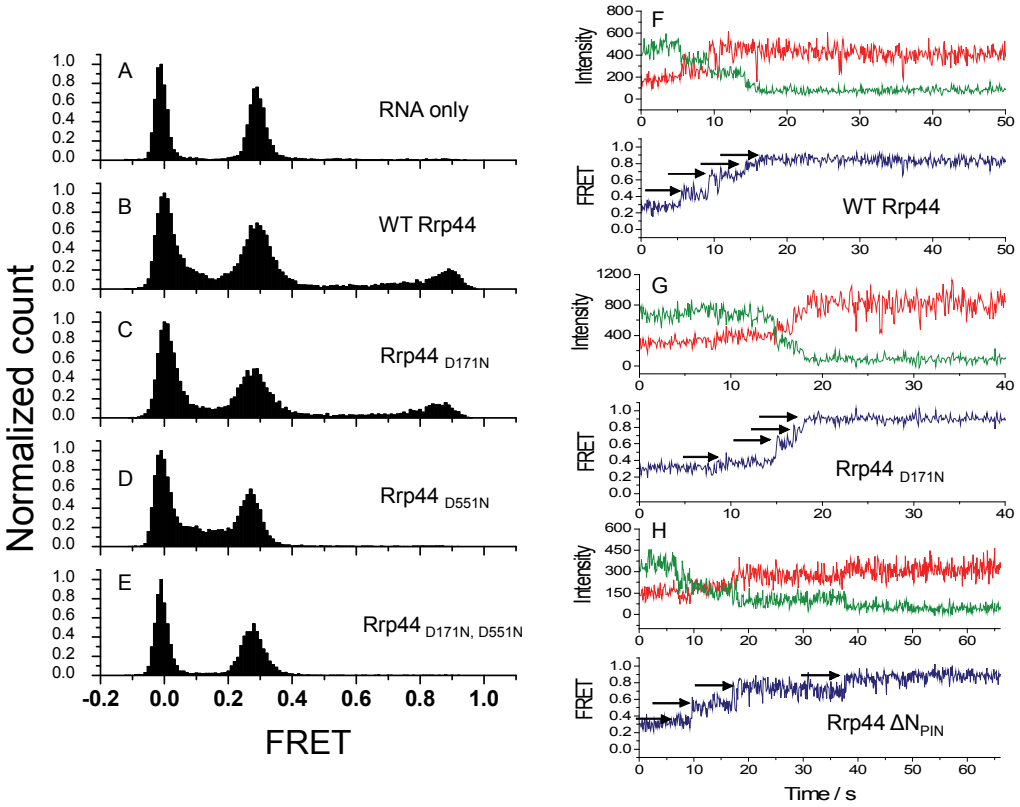

Fig. S2. The exonuclease activity of Rrp44 is responsible for the unwinding of dsRNA. The exonuclease of Rrp44 converts dsRNA to ssRNA via processive degradation, shifting the FRET population from 0.27 to 0.87. (A) Single molecule FRET efficiency histogram of the substrate only (60% GC content). The peak at FRET=0.29 represents the RNA substrate labeled with both the donor and the acceptor. The peak at FRET=0 represents the RNA substrates with the donor but with the acceptor missing or inactive. (B) FRET histogram 2 min after wild type Rrp44 was introduced. The peak at FRET=0.88 represents the degradation/unwinding product. (C) FRET histogram 2 min after $Rrp44_{D171N}$ (mutant at the active site of endonuclease) was introduced. A similar reaction amplitude was observed as in the wild type. We found that the overall unwinding time, defined as the time it takes for the FRET signal to change from the minimum to the maximum values, is about 25% longer for $Rrp44_{D171N}$ compared to the wild type. (D) FRET histogram 2 min after $Rrp44_{D551N}$ (mutant at the active site of exonuclease) was introduced. (E) FRET histogram 2 min after double mutant $Rrp44_{D171N, D551N}$ was introduced (mutations at both the active sites of endo- and exo-nuclease). The reactions using $Rrp44_{D551N}$ and $Rrp44_{D171N, D551N}$ do not show a degradation peak at FRET=~0.87 and their time traces did not show any evidence of RNA degradation. (F-H) Representative fluorescence intensity (top) and FRET efficiency (bottom) time trajectories of WT (F), $Rrp44_{D171N}$ (G) and Rrp44$\triangle N_{pin}$(H). The reaction yield of Rrp44$\triangle N_{pin}$ was low and the degradation products were not pronounced in its FRET efficiency histogram (not shown), but we typically obtained ~5-10 unwinding time traces per reaction. The low yield might originate from a weakened binding of the protein to RNA due to the deletion of the PIN domain.

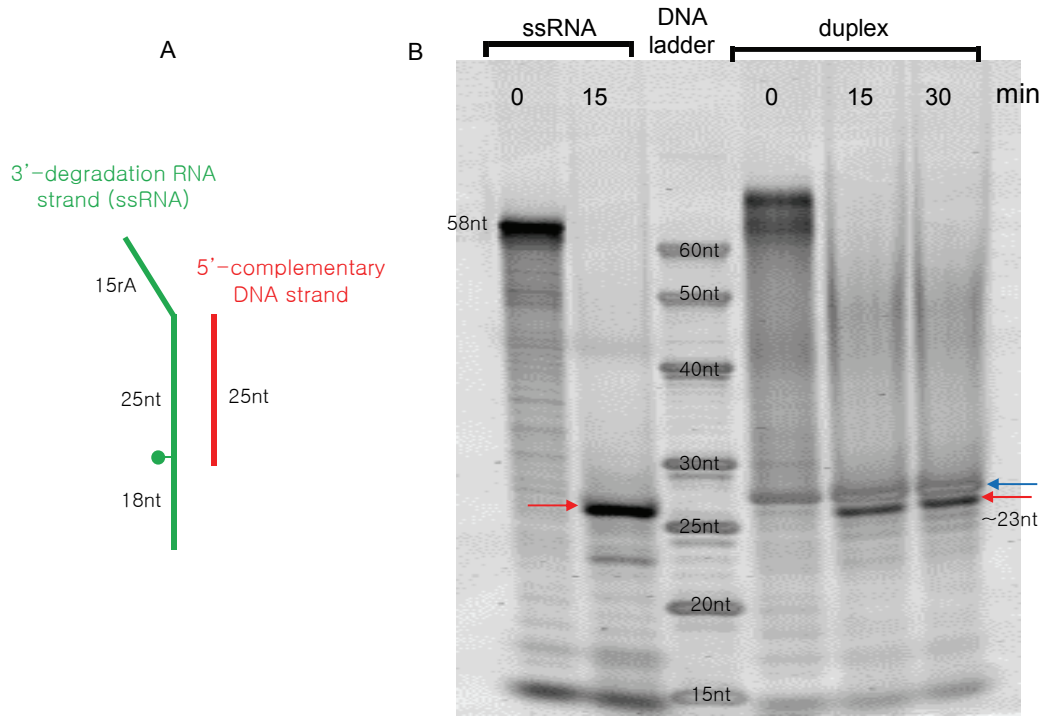

Fig. S3. Rrp44 unwinds and degrades fluorescently-labeled RNA substrates (A) Structure of the fluorescently labeled dsRNA substrate used for gel-based degradation assay. The green ball represents a Cy3 fluorophore conjugated through amino-dT. (B) Composite native gel image obtained via Cy3 fluorescence imaging and Sybr Gold staining of oligonucleotides. **lane 1**: 3' ssRNA alone, **lane 2**: 3' ssRNA incubated with Rrp44 for 15 min, **lane 3**: ssDNA ladder, **lane 4**: RNA-DNA hybrid alone, **lane 5-6**: the hybrid incubated with Rrp44 for 15 min and 30 min, respectively. The degradation products of the hybrid shown in lanes 5 and 6 (red arrows) appeared at the same position as that of lane 2 (red arrow), suggesting that the Rrp44 digested the 3' RNA strands to the same length in the context of an RNA duplex as in the context of a single stranded form. The bands in the lanes 4, 5, and 6 appearing right above the degradation product (blue arrows) were the 5' complementary DNA strands that were released after unwinding.

We found that RNA migrated slower than DNA (compare the lanes 1 and 3), and the modification for labeling also decreased the mobility of the oligos (note that the 25 nt DNA ladder strand in lane 3 migrates faster than the 25 nt DNA complementary strand (lines 4-6)without and with the modification, respectively, but they migrated at different speeds). Taken together, we estimated the degradation product length of the 3' RNA strand to be ~23 nt, which is ~5 nt away from Cy3, presumably due to a narrow entryway to the active site.

Experimental condition of RNA degradation assays:
For a degradation reaction ~100 pmol of RNA was mixed with ~25 pmol Rrp44 in 50 µl buffer solution containing 20 mM Tris, 10mM NaCl, 100 µM $MgCl_2$, and 100 µg/ml BSA (pH 7.8). The sample was incubated for different time courses in room temperature, and the reactions were

stopped by adding 50 μl of formamide. The reaction products were loaded and resolved on a native PAGE gel (20% polyacrylamide). The gel was treated with 1× SYBR Gold for 10 min to visualize the DNA ladder, and was imaged using a fluorescence imager (Typhoon, GE science).

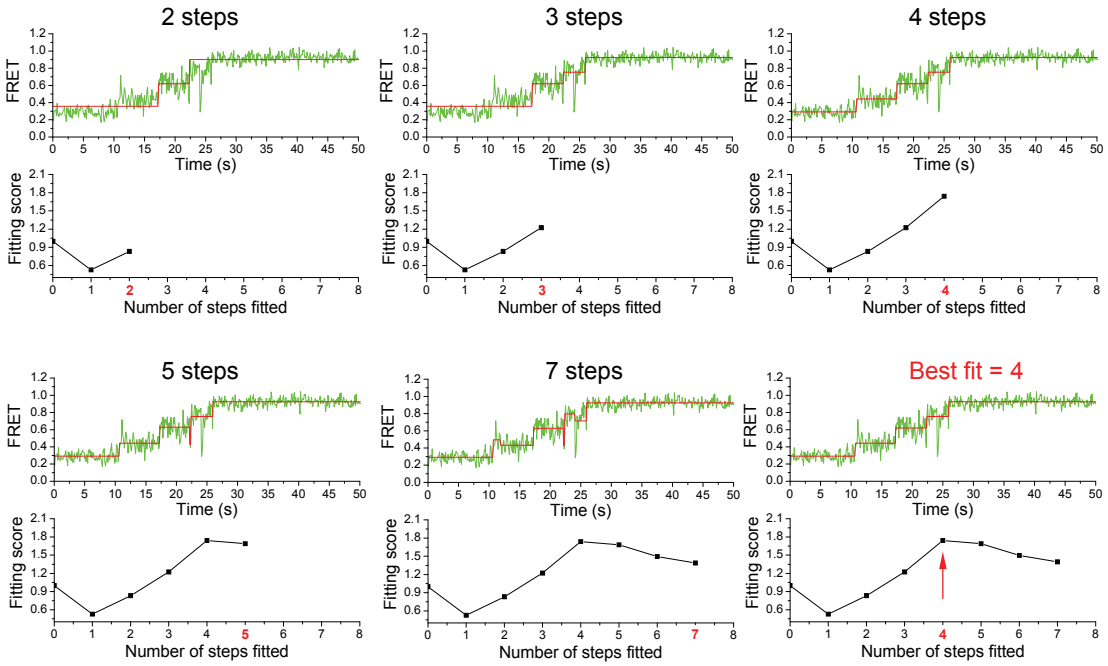

Fig. S4. Automated step finding algorithm. To obtain the FRET values of the steps from single molecule traces, we used a Matlab code to determine the most likely number of steps by fitting individual FRET traces obtained from unwinding reaction. The Matlab program was originally developed by Kerssemarkers *et al.* and was adopted by other studies (*9, 19*). The program fits the data from 1 step to 8 steps models and calculates the fitting score. A higher score represents a better fitting. The top panel of each graph shows the number of steps being fitted (FRET traces in green and fitting traces in red) while the bottom panel shows a progress of the fitting score as a function of increasing number of steps fitted. The algorithm yielded the highest score at the four steps. After the best fit is determined by the score, the fitting program provides all the information of duration of FRET value of each step. Histograms of FRET values and dwell times of each step can then be constructed.

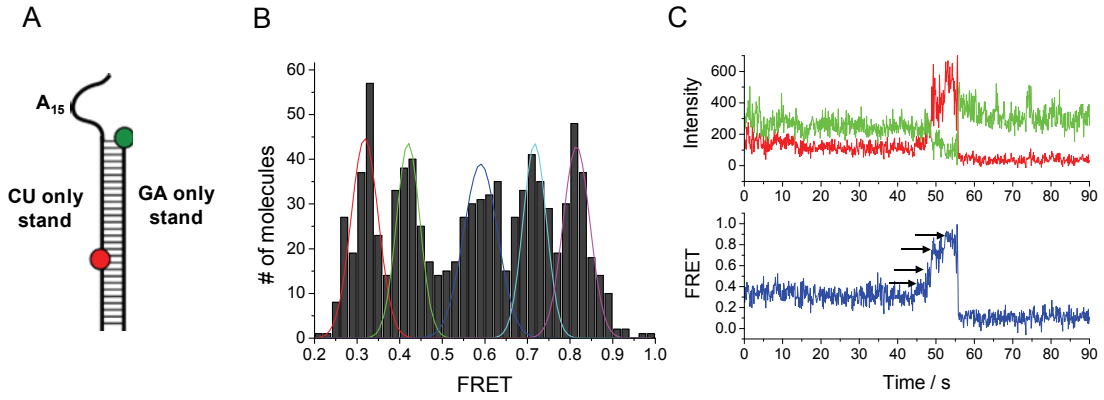

Fig. S5. The stepwise pattern does not originate from a secondary structure formation, indicating that the steps are intrinsic to the unwinding reaction and is not a sequence-specific feature. (A) The schematic of a redesigned RNA duplex in which the degradation strand (left black) consists of Cs and Us whereas its complementary RNA is composed of Gs and As so that they cannot form any secondary structure as the enzyme unwinds the duplex. (B) FRET histogram of unwinding steps. The FRET values of steps are slightly different from those of our standard construct, likely due to the difference in sequences. (C) A representative single molecule reaction shows donor and acceptor intensities (upper panel) and the corresponding FRET efficiency (lower panel). The sudden drop in FRET at ~56 s is due to acceptor phobleaching.

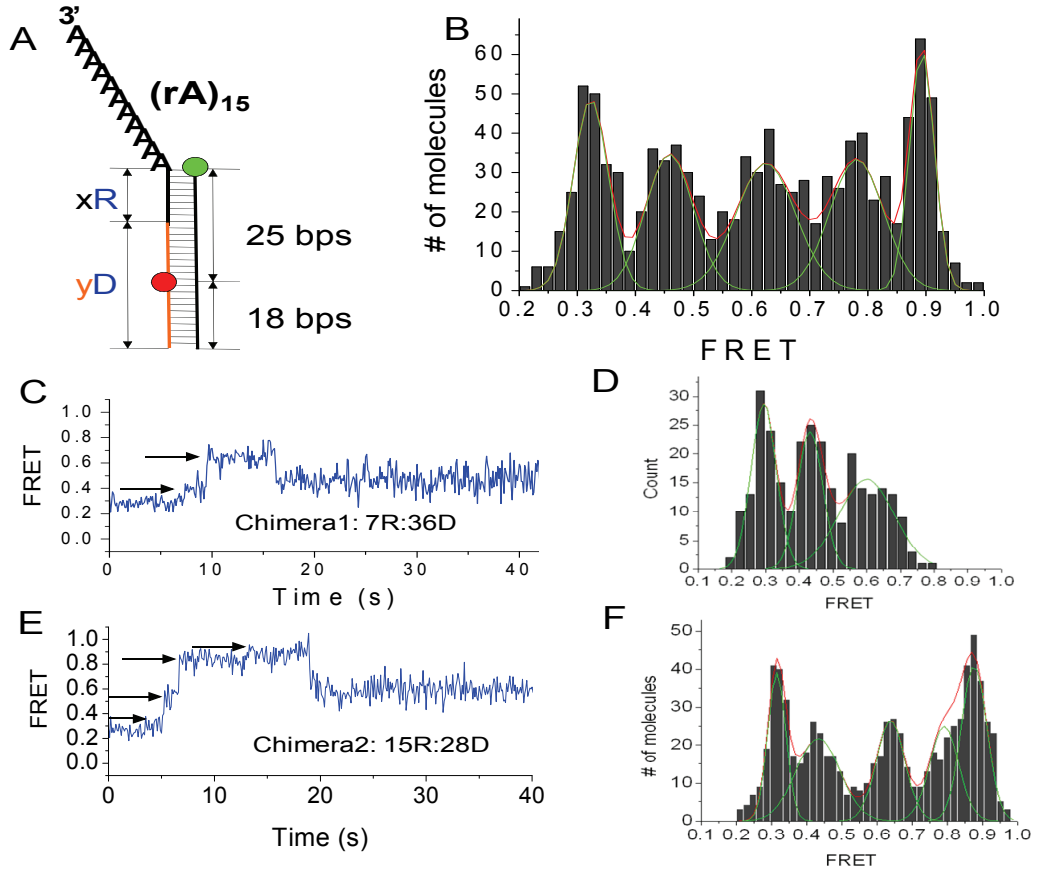

Fig. S6. Data with chimeric substrates suggest ~ 4 bp unwinding step size. (A) The schematic of calibration constructs. The substrate strand is a chimeric strand denoted by xR:yD, representing x nt of RNA (black) and y nt of DNA (orange) in the duplex. (B) The reference histogram of FRET efficiencies showing five peaks (four-stepped unwinding) observed from the all RNA substrate, reproduced here from Fig. 1D. (C) A representative time trace of FRET efficiency for Chimera1 (7R:36D) that has a RNA-DNA junction at 7 nt into the duplex. We generally observe two steps to reach the highest FRET value ~ 0.63 (black arrow) followed by a FRET decrease which we attribute to dissociation of the enzyme due to a lower affinity between the DNA strand that now occupies the entry tunnel of Rrp44. (D) Histogram of three FRET values obtained from Chimera1 (as marked by the black arrow in (C)). (E) A representative time trace of FRET efficiency for Chimera2 (15R:28D) that has a RNA-DNA junction at 15 nt into the duplex. We generally observed four steps to reach the highest FRET value ~ 0.87 (black arrow). (F) Histogram of five FRET values obtained from Chimera2 (as marked by the black arrow in (E)). The enzyme will stop at the chimeric junction because the enzyme cannot digest DNA. The difference of stalled positions between the two chimeric constructs is 8 bp and the difference in the number of steps is 4. Therefore, we estimate that the step size of unwinding is about 4 bp (=8/2). The data from chimeric constructs also suggest that in the standard all RNA construct, the FRET signal is insensitive to degradation much beyond 15 nt into the duplex.

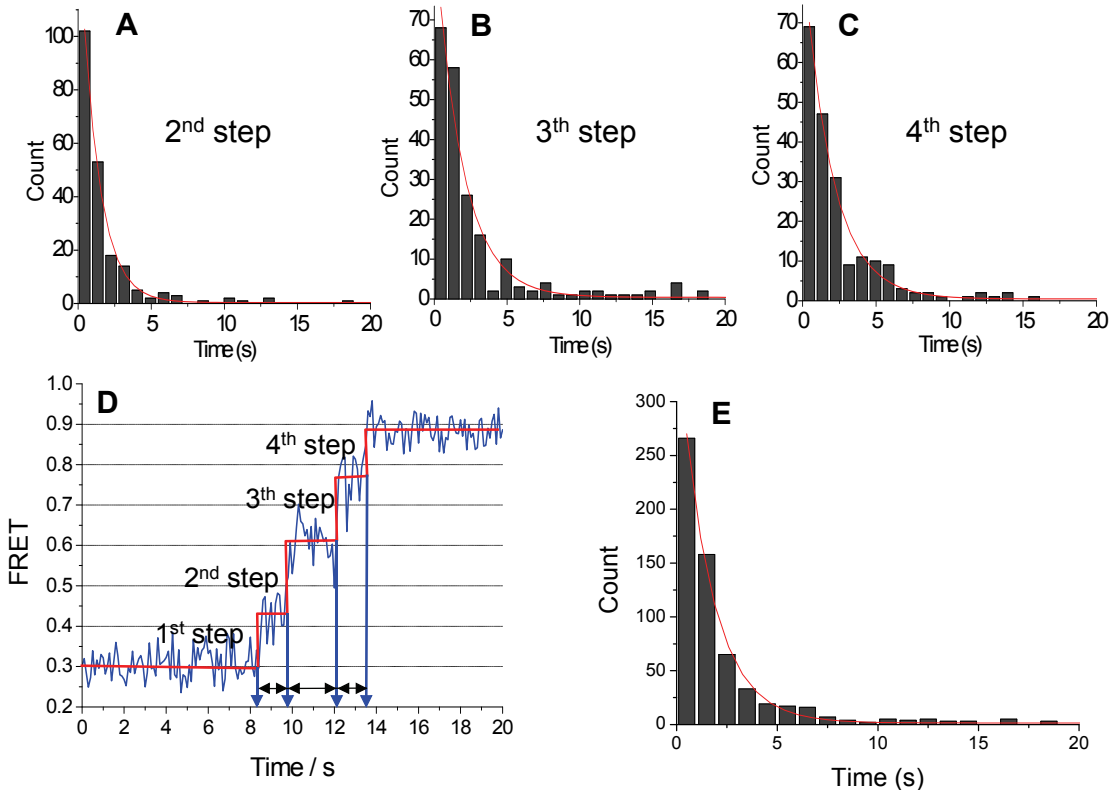

Fig. S7. Each unwinding step is exponentially distributed. The dwell time of each step (2nd, 3rd, and 4th steps) was determined from 209 molecules of the standard substrate (60% GC content) that showed 4 clear steps. The dwell times of the second to fourth steps were determined by the step finder algorithm based on sharp FRET changes whereas that of the first step was not analyzed due to the uncertainty of its starting point. (A-C) Histograms of dwell times (2 to 4 steps respectively) and exponential fits. The average lifetime determined from the exponential decay time is also shown. (D) Each black arrow corresponds to dwell time at each step. (E) A histogram of the dwell times collected from the last three steps (from 2 to 4 steps). The average dwell time of each unwinding step is ~1.6 s.

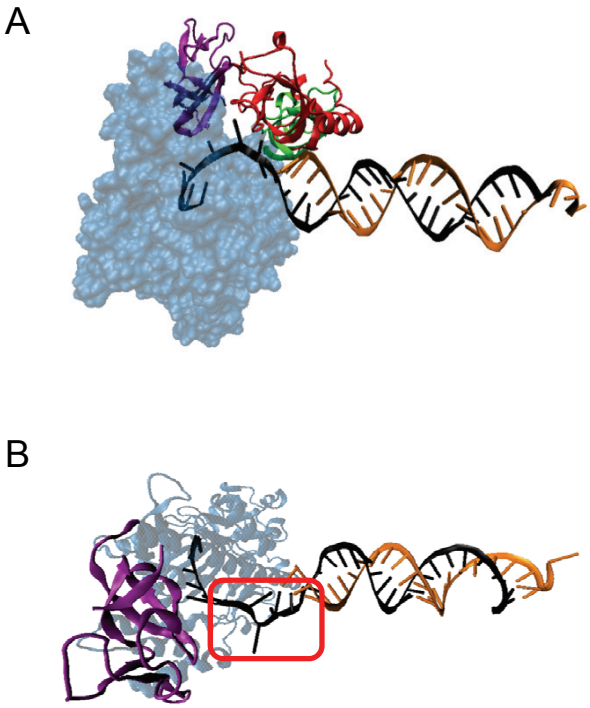

Fig. S8. CSD1 may interact with the 5' complementary strand, serving as an anchor domain. The crystal structures of yeast Rrp44 (PDB code: 2VNU) (*6*) and double stranded siRNA (PDB code: 2F8T) (*32*) are assembled *in silico* to examine the possible interaction between dsRNA and domains of the protein. The domains of S1, RNB, CSD1 and CSD2 are colored in purple, blue, green, and red, respectively. (A) A dsRNA co-crystallized with Argonaute (ref. S5) is connected to the ssRNA co-crystallized with the Rrp44. The reconstructed structure shows that the CSD1 (red) situates near to the 5' complementary strand (orange), showing a putative interaction between the CSD1 and the 5' complementary strand of the duplex. The CSD1 and RNB domains may serves as two anchor regions as suggested for RNaseII (ref. S(*5*). The interactions in both anchor regions may enable the enzyme to accumulate elastic energy while preventing thermal fraying. (B) The flexible ssRNA bridging both the catalytic RNB and CSD1 domains (red box) could be stretched during a series of degradation steps, resulting in a tension in the RNA/protein complex.

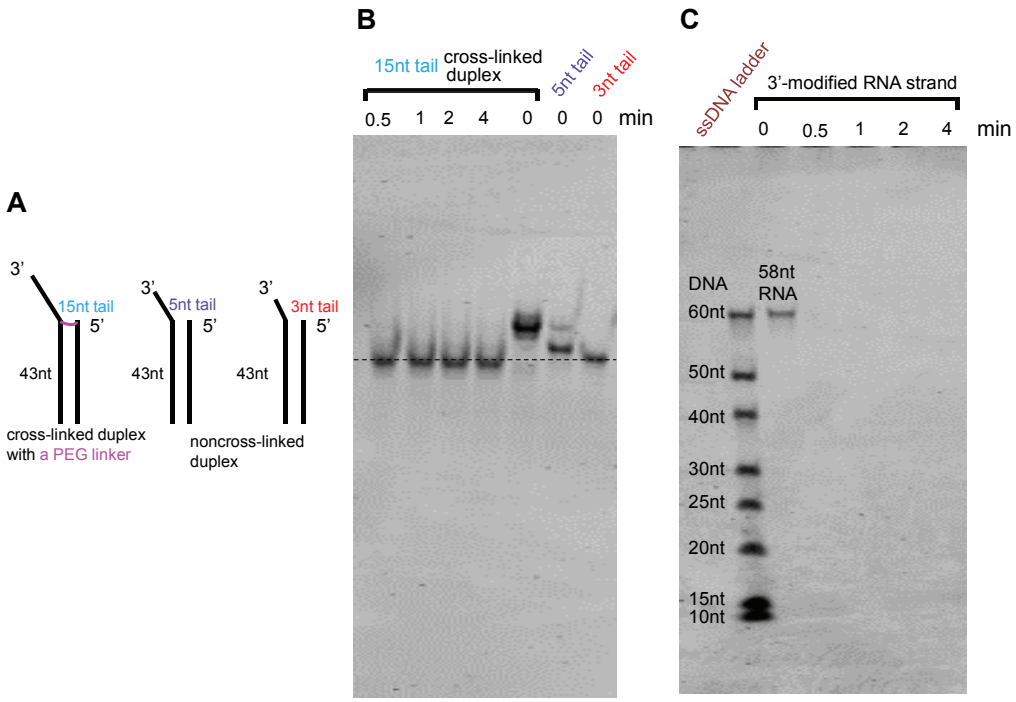

Fig. S9. Rrp44 can digest the 3' tail down to ~3 nt without duplex unwinding.
(A) We made a construct where the two strands are cross-linked at the ss-ds junction by a $[PEG]_4$ linker targeting an amino-modification on the 5' substrate RNA strand and a thiol modification on the 3' complementary DNA strand. This construct allowed us to test how close the enzyme's active site can come toward the duplex without duplex unwinding. Also shown are the calibration constructs of RNA duplexes of the same length with a 5 or 3 nt 3' tail.

(B) Lanes 1-4 of the native gel show the degradation time course of the cross-linked construct. Lane 5 is the untreated cross-linked construct whereas lanes 6 and 7 are calibration constructs with 5 nt and 3 nt tails, respectively. The migration profile of the crosslinked construct treated with Rrp44 is similar to that of the 3nt calibration, suggesting that a significant stretching of the single strand RNA or compression of the enzyme compared to what was seen the ssDNA/Rrp44 co-crystal structure which showed that 7 nt of ssRNA is necessary to reach the active site.

(C) To confirm that inability of Rrp44 to degrade the 3' substrate beyond ~3 nt overlang is caused by cross-linking, not the amino-modification itself, we incubated Rrp44 with the 3' strand for different durations. The 3' strand was completely degraded even after 0.5 min reaction (lanes 3-6).

Experimental condition of RNA degradation assays:
The 3' stand with an amino modification was purchased from Dharmacon® and the 5' stand with a thio modification was purchased from IDT DNA® (see RNA substrate preparation in Material and Methods for more details). The RNA cross-linking reaction was performed following the manufacturer's instructions (Thermo Scientific: product # 22107). For a degradation reaction

~10 pmol of RNA was mixed with ~25 pmol Rrp44 in 50 μl buffer solution containing 20 mM Tris, 10mM NaCl, 100 μM $MgCl_2$, and 100 μg/ml BSA (pH 7.8). The sample was incubated for different durations in room temperature, and the reactions were stopped by adding 50 μl of formamide. The reaction products were loaded and resolved on a native PAGE gel (15% polyacrylamide). The gel was treated with 1× SYBR Gold for 20 min to visualize RNA and the DNA ladder, and was imaged using a fluorescence imager (Typhoon, GE science).

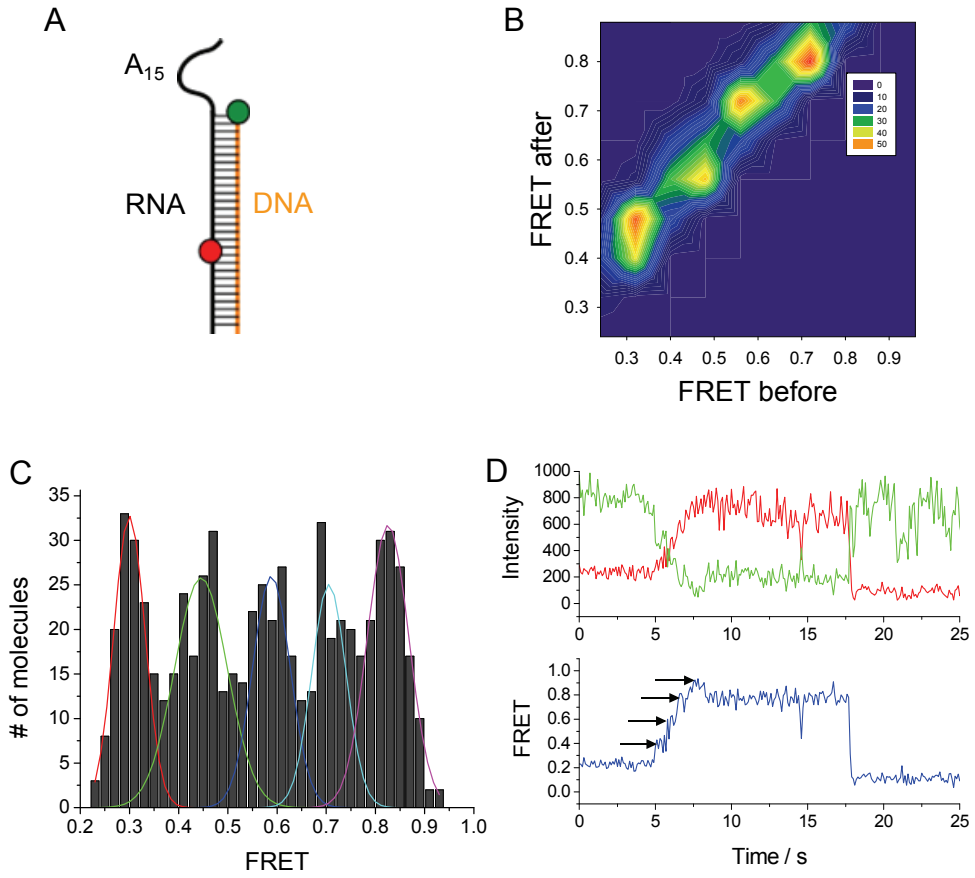

Fig. S10. The RNA/DNA hybrid shows the four-stepwise pattern similar to the RNA/RNA duplex. (A) The schematic of the heteroduplex in which the substrate strand (black) is the same RNA as the one used in Fig. 1F whereas its complementary strand (orange) is made of DNA. (B) Transition density plot collected from 137 molecules of the RNA-DNA heteroduplex construct shows the two-dimensional density plot of FRET values before and after each step. Four discrete clusters demonstrate that there are four steps occurring through well-defined FRET values. (C) FRET histogram of pause-steps. (D) A representative set of time traces of fluorescence intensities and FRET efficiency.

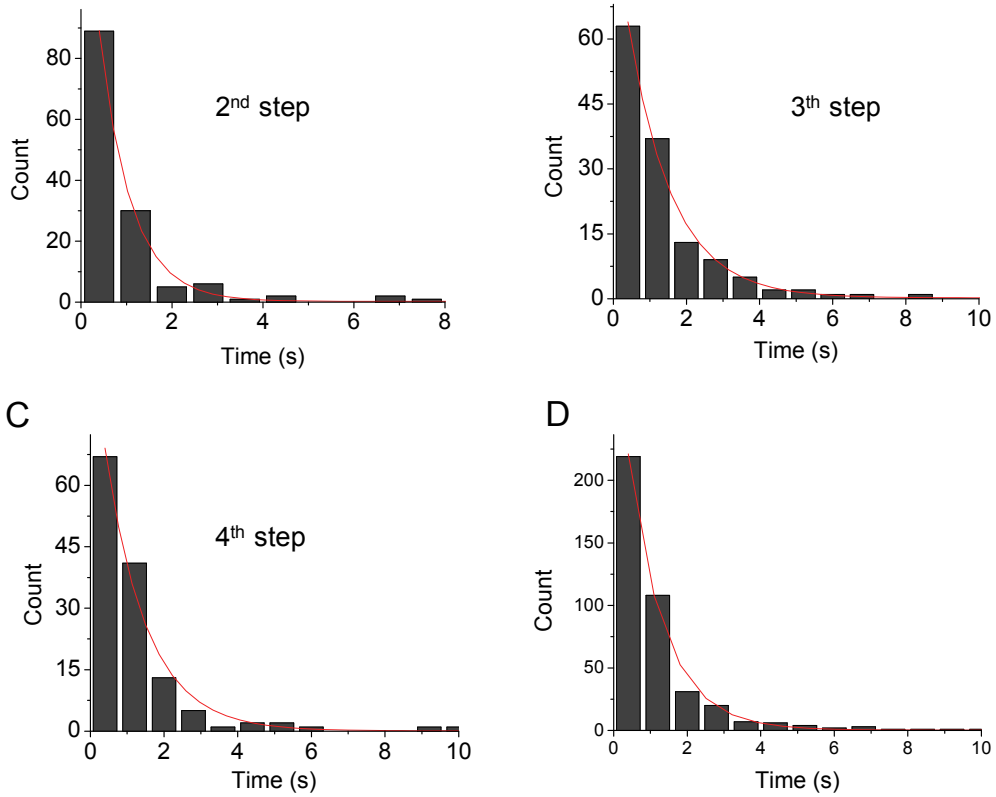

Fig. S11. Rrp44 unwinds the RNA-DNA heteroduplex 60% faster than RNA-RNA duplex with the same sequence. The RNA-DNA heteroduplex was prepared by annealing two strands: the 3' substrate strand (the same strand in Fig.1F) and its complementary DNA strand. (A-C) Histograms of dwell times of 2nd, 3rd, and 4th steps, respectively) and exponential fits. (D) The exponential fit of all the dwell times collected from all three steps gives ~1s which is 60 % shorter than that of the RNA-RNA duplex (Fig. S7).

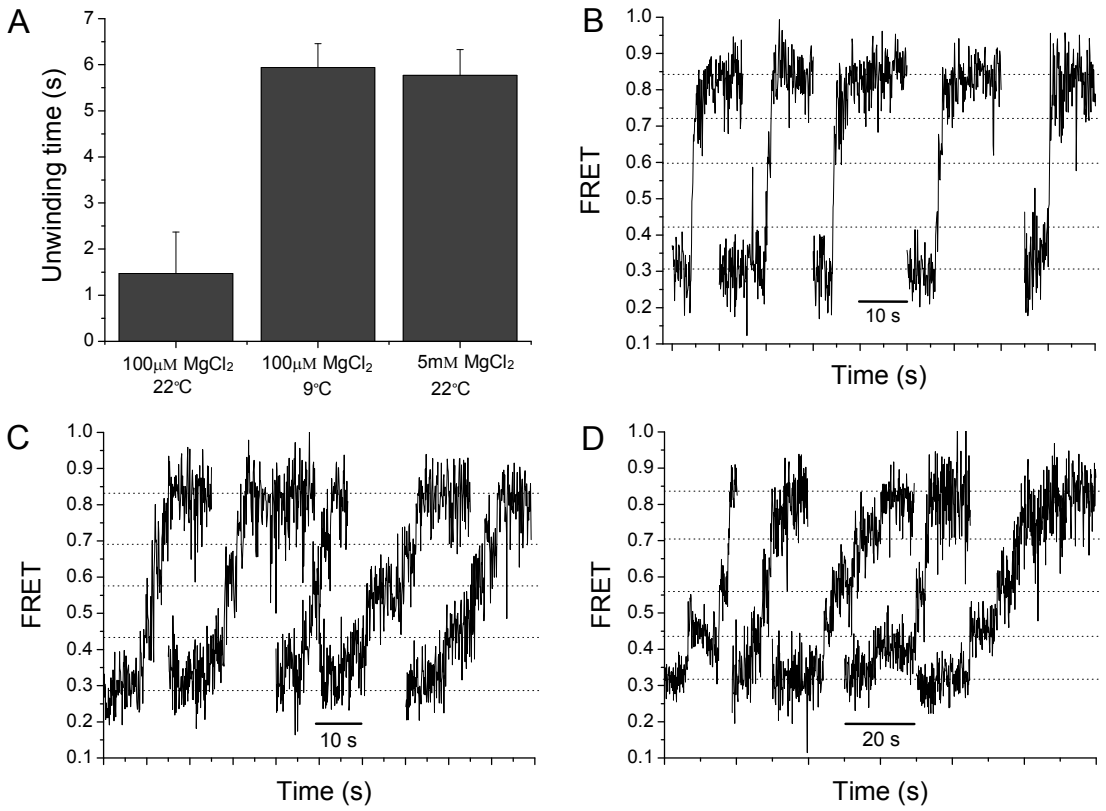

Fig. S12. The overall reaction time is determined by duplex stability and temperature. (A) A comparison of unwinding times of the AU-rich construct at different temperatures and Mg^{2+} concentrations. Unwinding is defined as the time it takes for FRET values to increase from the initial low value to the highest final state. (B) Representative FRET traces obtained in 100 μM $MgCl_2$ at room temperature (23 ˚C). Unwinding of the AU-rich construct was too fast to resolve the steps. (C) Representative FRET traces obtained in 100 μM $MgCl_2$ at 9˚C. (D) Representative FRET traces obtained in 5 mM $MgCl_2$ at room temperature.

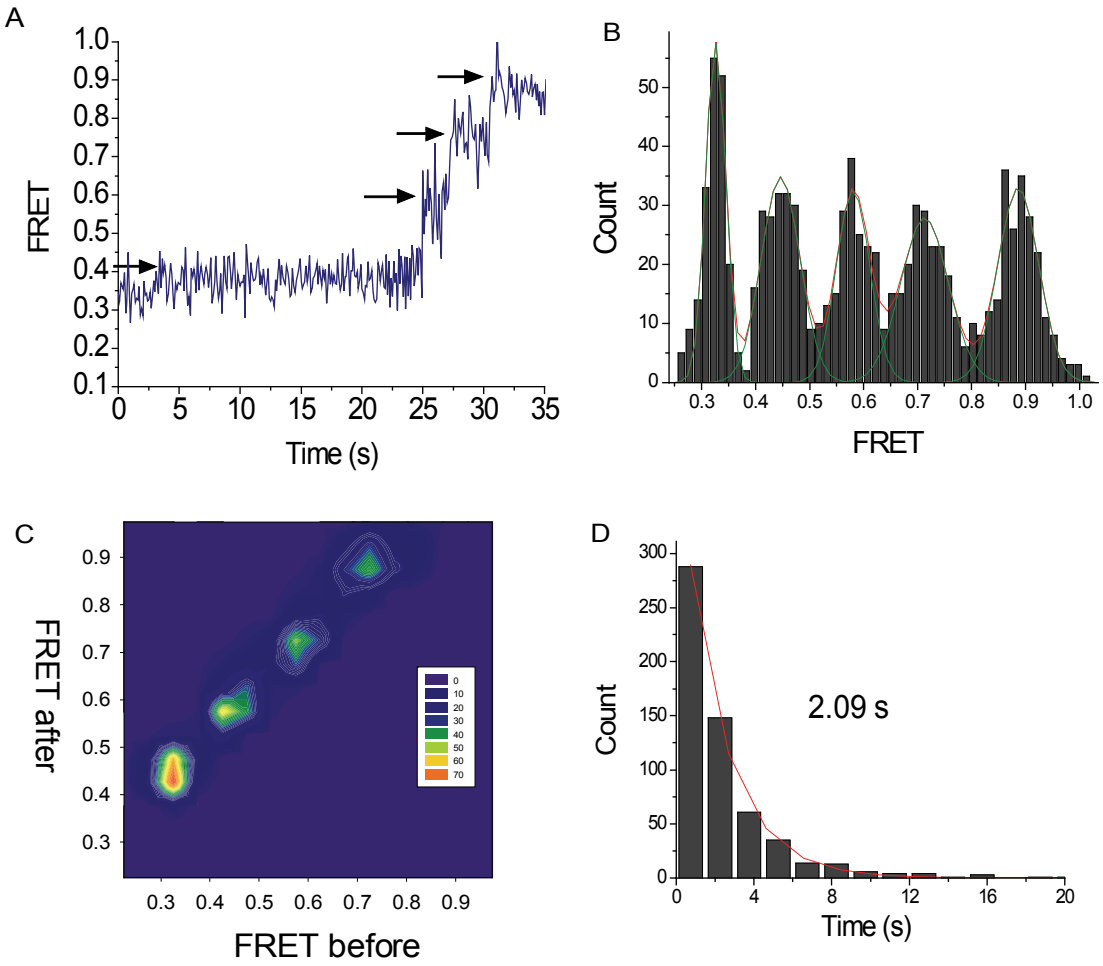

Fig. S13. ***E. coli*** **RNaseR displays stepwise unwinding during degradation of the standard RNA duplex.** (A) Representative FRET traces obtained from RNaseR in 5mM $MgCl_2$ at ~12˚C. (B) Distribution of each FRET state visited during unwinding (197 molecules). Four steps were observed (five different FRET values) at similar FRET values observed for Rrp44, suggesting a similar step size of unwinding . (C) 2-Dimensional FRET histogram of pause-steps determined by FRET changes before and after transitions. (D) A histogram of the dwell times collected from the last three steps (from 2 to 4 steps) shows a single exponential decay. The average dwell lifetime of each unwinding step is ~2.1 s. Interestingly, a study has reported that RNase R active site mutants have an unwinding activity on a short duplex at a micro-molar protein concentration in the presence of ATP (*33*). Our data on Rrp44 and RNase R were obtained without ATP and we did not observe any unwinding-like signal from various Rrp44 exonuclease mutants on several 48 bp duplex constructs.

References

1. J. Houseley, J. LaCava, D. Tollervey, Nature Reviews Molecular Cell Biology 7, 529 (2006).
2. S. Vanacova, R. Stefl, Embo Reports 8, 651 (2007).
3. A. Lebreton, R. Tomecki, A. Dziembowski, B. Seraphin, Nature 456, 993 (2008).
4. D. Schaeffer et al., Nature Structural & Molecular Biology 16, 56 (2009).
5. C. Frazao et al., Nature 443, 110 (2006).
6. E. Lorentzen, J. Basquin, R. Tomecki, A. Dziembowski, E. Conti, Molecular Cell 29, 717 (2008).
7. A. Dziembowski, E. Lorentzen, E. Conti, B. Seraphin, Nature Structural & Molecular Biology 14, 15 (2007).
8. J. A. Ali, T. M. Lohman, Science 275, 377 (1997).
9. S. Myong, M. M. Bruno, A. M. Pyle, T. Ha, Science 317, 513 (2007).
10. A. Schwartz et al., Nature Structural & Molecular Biology 16, 1309 (2009).
11. W. Cheng, S. G. Arunajadai, J. R. Moffitt, I. Tinoco, Jr., C. Bustamante, Science 333, 1746 (2011).
12. J. Y. Lee, W. Yang, Cell 127, 1349 (2006).
13. T. Ha et al., Proceedings Of The National Academy Of Sciences Of The United States Of America 93, 6264 (1996).
14. M. C. Murphy, I. Rasnik, W. Cheng, T. M. Lohman, T. J. Ha, Biophysical Journal 86, 2530 (2004).
15. S. X. Liu, E. A. Abbondanzieri, J. W. Rausch, S. F. J. Le Grice, X. W. Zhuang, Science 322, 1092 (2008).
16. G. Lee, J. Yoo, B. J. Leslie, T. Ha, Nature Chemical Biology 7, 367 (Jun, 2011).
17. Among all FRET traces obtained, more than 45 % traces shows four apparent steps. The step analysis suggests that the most of the rest of traces also may have a four step behavior but some of them are sometimes missing because they are faster than our time resolution (Fig. S2).
18. G. Lee, S. Hartung, K. P. Hopfner, T. Ha, Nano Letters 10, 5123 (2010).
19. J. W. J. Kerssemakers et al., Nature 442, 709 (2006).
20. S. A. McKinney, C. Joo, T. Ha, Biophysical Journal 91, 1941 (2006).
21. E. A. Lesnik, S. M. Freier, Biochemistry 34, 10807 (1995).
22. R. E. Dickerson et al., Science 216, 475 (1982).
23. M. S. Z. Kellermayer, S. B. Smith, H. L. Granzier, C. Bustamante, Science 276, 1112 (1997).
24. Y. Seol, G. M. Skinner, K. Visscher, A. Buhot, A. Halperin, Physical Review Letters 98, (2007).
25. H. W. Wang et al., Proceedings of the National Academy of Sciences of the United States of America 104, 16844 (2007).
26. F. Bonneau, J. Basquin, J. Ebert, E. Lorentzen, E. Conti, Cell 139, 547 (2009).
27. R. Tomecki et al., Embo Journal 29, 2342 (2010).
28. J. R. Moffitt et al., Nature 457, 446 (2009).
29. A. Revyakin, C. Y. Liu, R. H. Ebright, T. R. Strick, Science 314, 1139 (2006).
30. A. N. Kapanidis et al., Science 314, 1144 (2006).
31. Single-Molecule Techniques: A Laboratory Manual. P. R. Selvin, T. Ha, Eds., (Cold Spring Harbor Laboratory Press, ed. 1), vol. 1.

32. Y. R. Yuan, Y. Pei, H. Y. Chen, T. Tuschl, D. J. Patel, Structure 14, 1557 (2006).
33. N. Awano et al., J Bacteriol 192, 1344 (2010).